Estimation of Particulate Organic Carbon Flux with BGC-Argo Backscatter data from the western North Pacific

Honda, M. C., T. Fujiki, S. Hosoda (JAMSTEC)
Y. Mino (Nagoya Univ.)
N. Harada (Univ. Tokyo)

hondam@jamstec.go.jp

1. Introduction
2. BGC-Argo floats
3. Backscatter vs POC concentration
4. Water Temperature
5. Chl-a
6. POC concentration
7. POC Inventory
8. Backscatter-based POC flux
9. Sediment trap-based POC flux at K1 and KEO
10. Summary

1. Introduction

For the sake of understanding the ocean's ability for uptake of atmospheric CO_2 and predict its future change by the change of the global/ocean environment, the biological carbon pump (BCP) should be quantified precisely. The study of the BCP has been conducting by, mainly, time-series sediment trap observation. In the 21century, the global observation network of the Argo floats has been established. Recently, fluorometer, pH sensor, nitrate sensor and backscatter meter can be installed on the Argo float. The Argo float equipped with these sensors (BGC- Argo) have enabled us to study the various biogeochemical oceanography. Among these sensors, the backscatter meters can observe spatial-temporal variability of marine particles in the water column and, thus, these data possibly contribute to the BCP study. After 2017, the BGC- Argo floats have been deployed at time-series stations (K2 and KEO) in the western North Pacific. Backscatter data observed during years of 2017-2020 in the subarctic region (SA) and of 2019-2021 in the subtropical region (ST) were converted to particulate organic carbon (POC) concentration data with the empirical equation and, sequentially, temporal variability in vertical profile of POC upper 1000 m were analyzed. Consequently, assuming the steady state and that lateral transport of POC are negligible, annual amplitude of POC inventory at respective depth was regarded as POC flux at respective depth.

2. BGC-Argo floats

Two BGC-Argo floats were deployed in the western North Pacific. The floats were equipped with a CTD sensor and a bio-optical sensor (ECO FLBB, WET Labs) to measure chlorophyll- a (Chl-a) fluorescence and particulate backscattering at 700 nm.

One (#2903210) was deployed at SA time-series station K2 in July 2017 (Table 1). Although this BGC-Argo drifted northward by about 52° N after deployment, this float stayed within the Western Pacific Subarctic Gyre (WSAG) for about three years (Fig. 1a). Thus, it can be said that this BGC-Argo data, in general, represents the oceanography for the WSAG.

Another float #2903394 was deployed at ST time-series station KEO in May 2019. After deployment, this float drifted westward and was trapped by the Kuroshio main stream (Fig. 1b). Sequentially, this float drifted westward along with the. In November 2020, this float arrived at 172Kuroshio extension° E. Thereafter, this float drifted westward and finally drifted north of 40° N. Thus, data does not always represent oceanography at around station KEO and, instead, represents that for the Kuroshio extension.

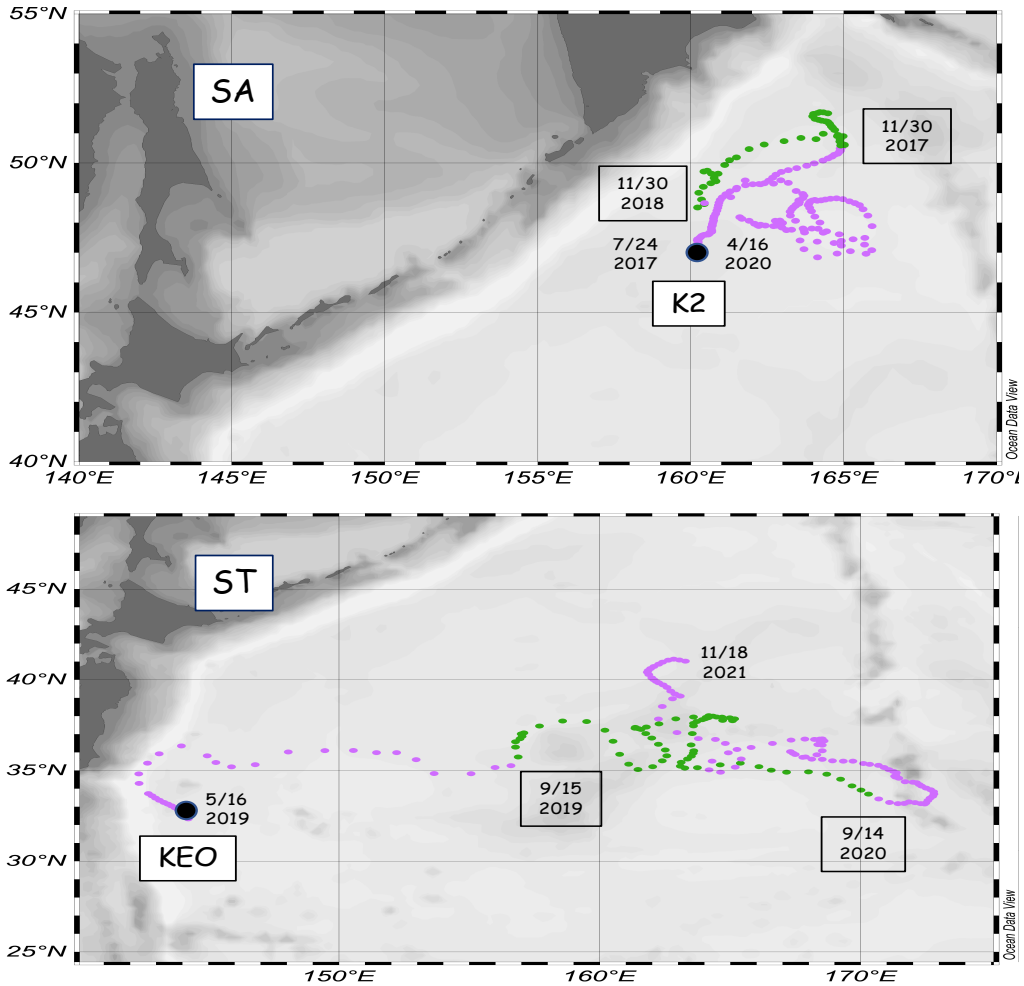

Figure 1 Drifting track of BGC-Argo floats for the western Pacific (a) subarctic and (b) subtropical regions. Annual POC fluxes were estimated with data from green positions.

3. Backscatter vs POC concentration

In order to propose the appropriate empirical equations for SA and ST regions this study, a several hundred seawaters at several depths were filtrated by using in situ filtering system (McLane WTS-6-1-142, USA) when BGC-Argo floats were deployed at both stations and POC concentrations were measured by using the elemental analyzer (Perkin-Elmer 2400 CHN/O, USA) at land laboratory. As a result, POC concentration (POC conc.: mg m^{-3}) and backscatter at 700 nm ($b_{bp(700)}$: m^{-1}) significantly correlated well at both regions (Fig. 2)

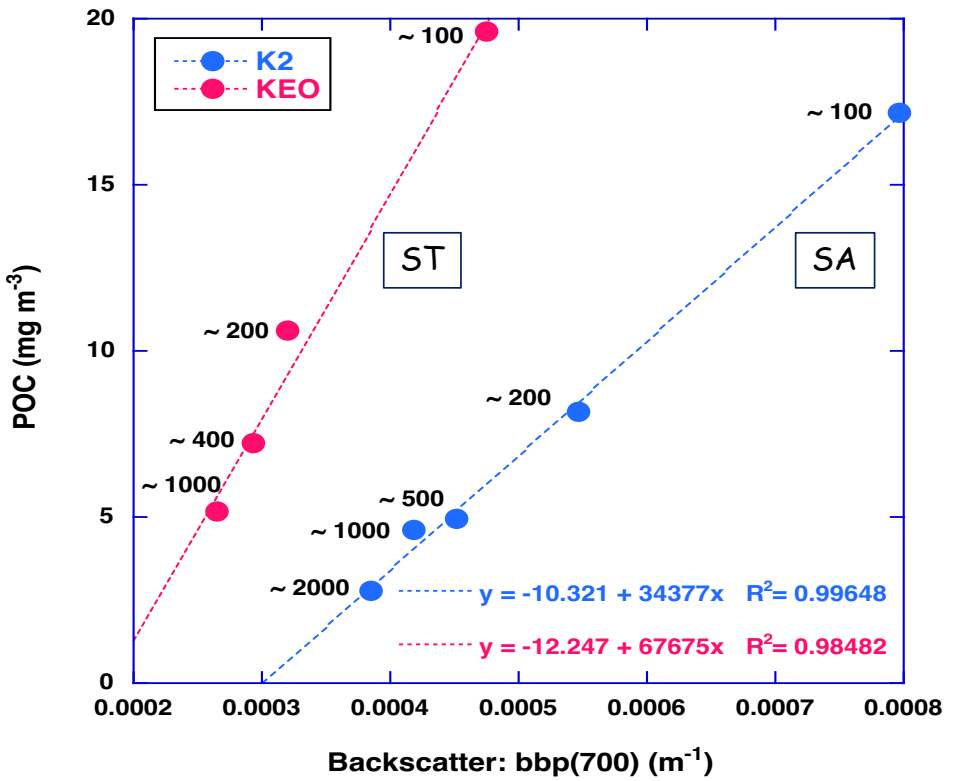

Figure 2 Relations between backscatter at 700 nm and POC concentration at stations K2 (red) and KEO (blue) observed when BGC-Argo floats were deployed at respective stations. Numbers in figure are water depth.

4. Water temperature

(SA) Sea surface temperature (SST) became the annual minimum of approximately 2° C in March (experimental days of ~ 250; ~ EXD250, ~ EXD600) and the annual maximum of 15° C in August (~ EXD400, ~ EXD750) (Fig. 3a). Below 150 m, significant seasonal variability in water temperature were not observed. Surface mixed layer depth, which is defined as depth with 0.125 higher density than shallowest (~ 5m) density, deepened by ~ 130 m in March and shallowed by ~ 15 m in August. In general, the period between January and May (July and September) was mixing season (stratified season).

(ST) Although water temperature was observed at different places, SST tended to become the annual maximum of ~ 27° C in August (~ EXD100, ~ EXD450, ~EXD800) and the annual minimum of ~ 15° C in February (~EXD250, ~EXD650) (Fig. 3b). Based on about one year and half observation, surface mixed layer was thin (~ 5m) in August (~EXD75 and ~ EXD450) and thick (~ 200 m) in February (~ EXD250). It is noteworthy that significant seasonal variability in water temperature was observed at around 500 m.

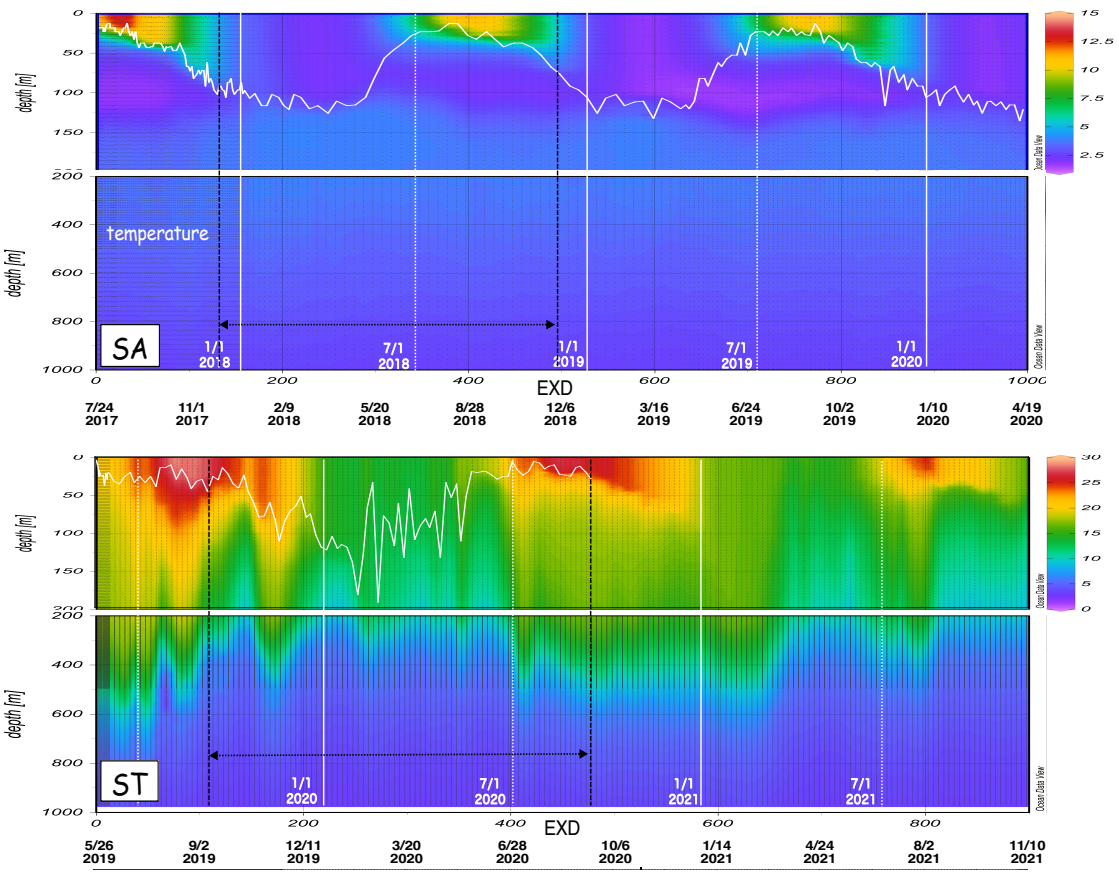

Figure 3 Profile time-series of water temperature for (a) subarctic (SA) and (b) subtropical (ST) regions. EXD is experimental days from the day when the first data was obtained. White solid line denotes surface mixed layer. Black broken arrow denotes the period when annual POC flux was estimated.

5. Chl-a

(SA) Chl-a upper 50 m started to increase in May (~ EXD300, ~ EXD650) (Fig. 4a). This is the typical "spring bloom" in the WSAG (K2). This spring bloom ceased in August or September (~ EXD400, ~ EXD750). However, Chl-a increased again in October and November. This is called "autumn bloom". During winter mixing period (December and April), Chl-a concentration was generally low.(Fig. 4a).

(ST) It is noteworthy that subsurface Chl-a maximum (SCM) appeared between ~ 50 and ~ 100 m during June (~ EXD0, ~ EXD400, ~ EXD750) and November (~ EXD150) or December (~ EXD550) (Fig. 4b). This SCM was also observed at former ST station S1. High Chl-a concentration upper 50 m was generally observed between March and June. During winter mixing period (January and March), Chl-a was low and this low Chl-a seawater extended to about 200 m.

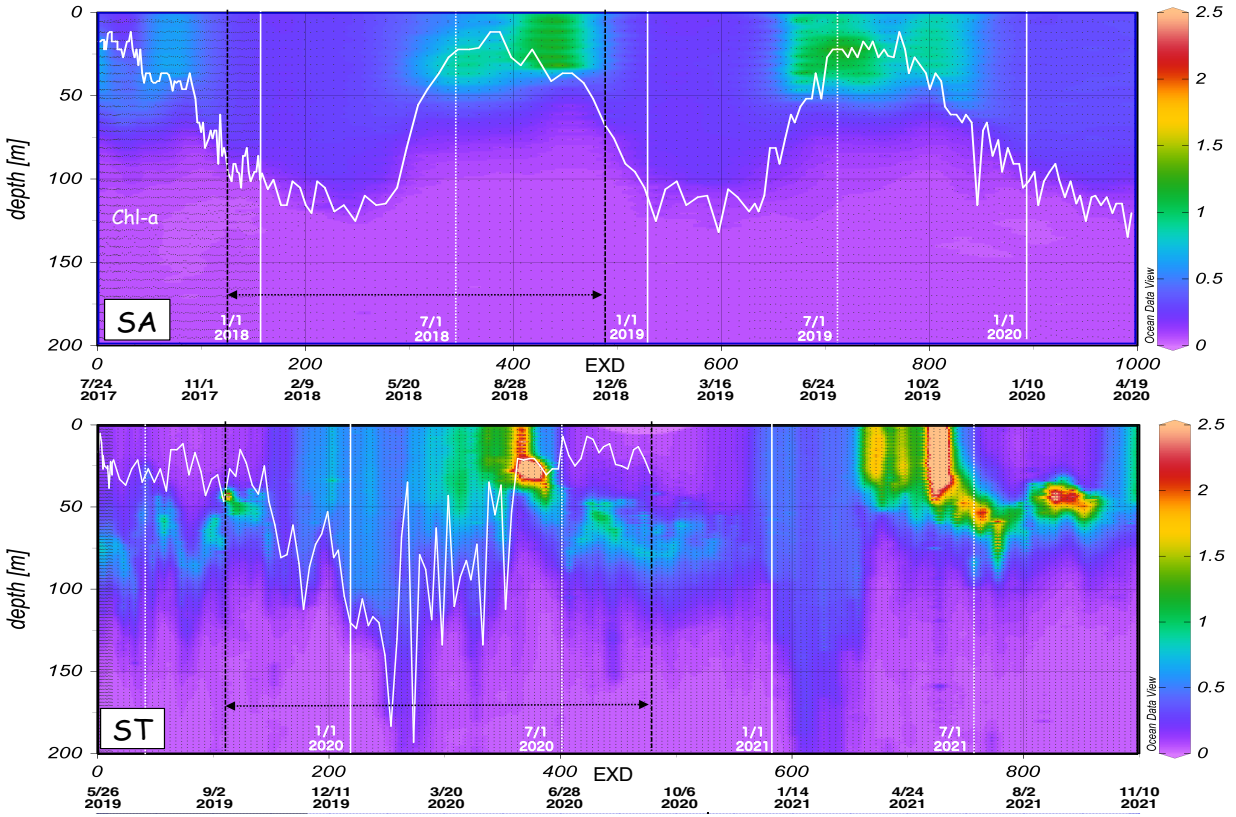

Figure 4 Same as Figure 3 except Chl-a and upper 200 m.

6. POC concentration

(SA) Seasonal variability in backscatter-based POC concentration for the WSAG upper 150 m was generally similar to that in Chl-a concentration: POC increased during the spring boom and autumn bloom and decreased during winter mixing period (Fig. 5a). Relatively high POC concentration appeared ubiquitously below 200 m during the spring bloom (~ EXD320) and autumn bloom (~ EXD450) .

(ST) Upper 200 m, seasonal variability in POC distribution was generally similar to that in Chl-a: POC concentration upper 50 m was observed between March / April and June, and relatively high POC concentration was observed at subsurface layer between July and December. During winter mixing period, lower POC concentration water extended to deeper than 200 m.

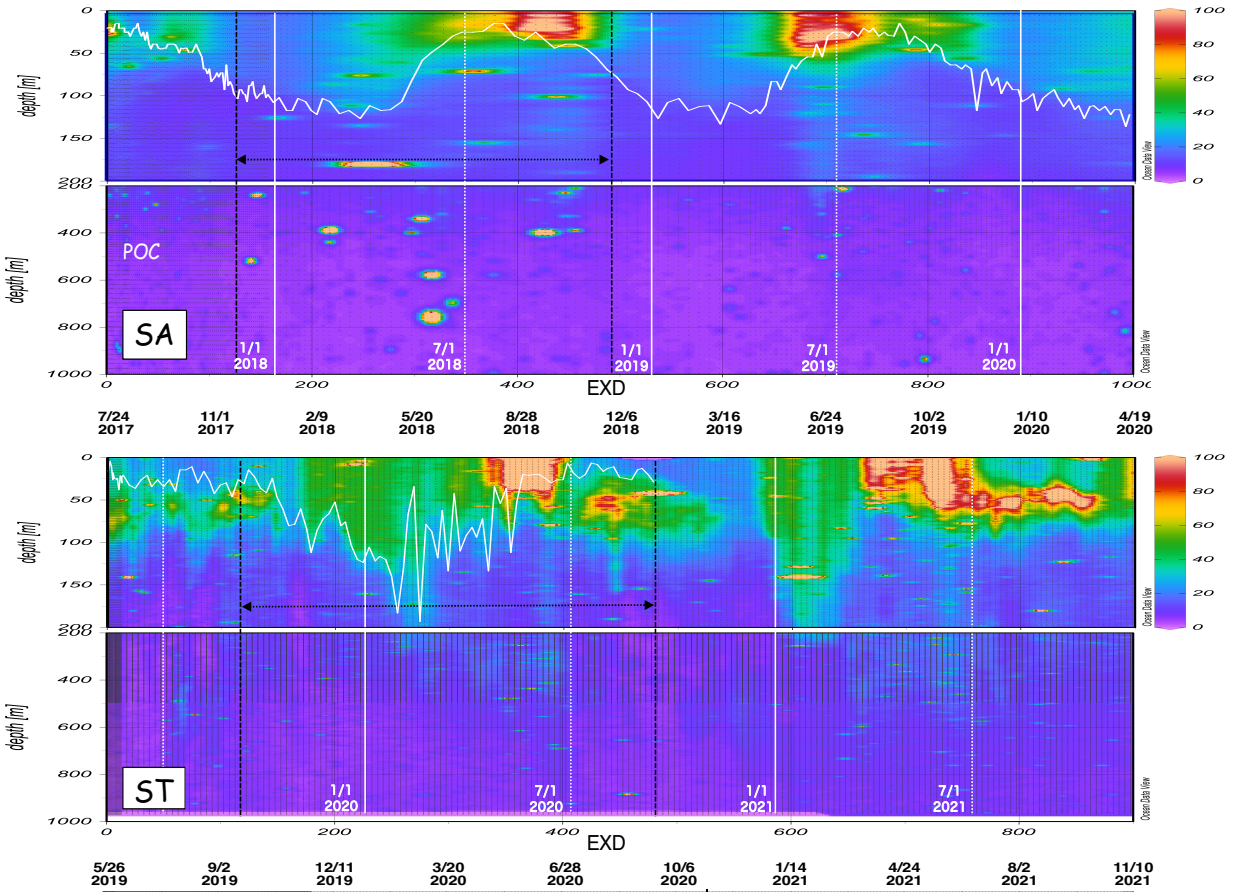

Figure 5 Same as Figure 3 except POC concentration.

7. POC inventory

Using vertical profile of backscatter-based POC concentration for respective measurements, POC inventories between multiple depths below 150 m for the SA region (200 m for the ST region) and reference depth (1000 m) were computed (Fig. 6).

In the SA region, POC inventory between 150 - 1000 m tended to become low in December (experimental day of 150: EXD150 and EXD500) and high in June (EXD330 and EXD700) (Fig. 6a). POC inventory and annual amplitude decreased with depth.

In the ST region, POC inventory became annual minimum in November 2019 (EXD175) and October 2020 (EXD500) and annual maximum in June (EXD400 and EXD750) (Fig. 6b).

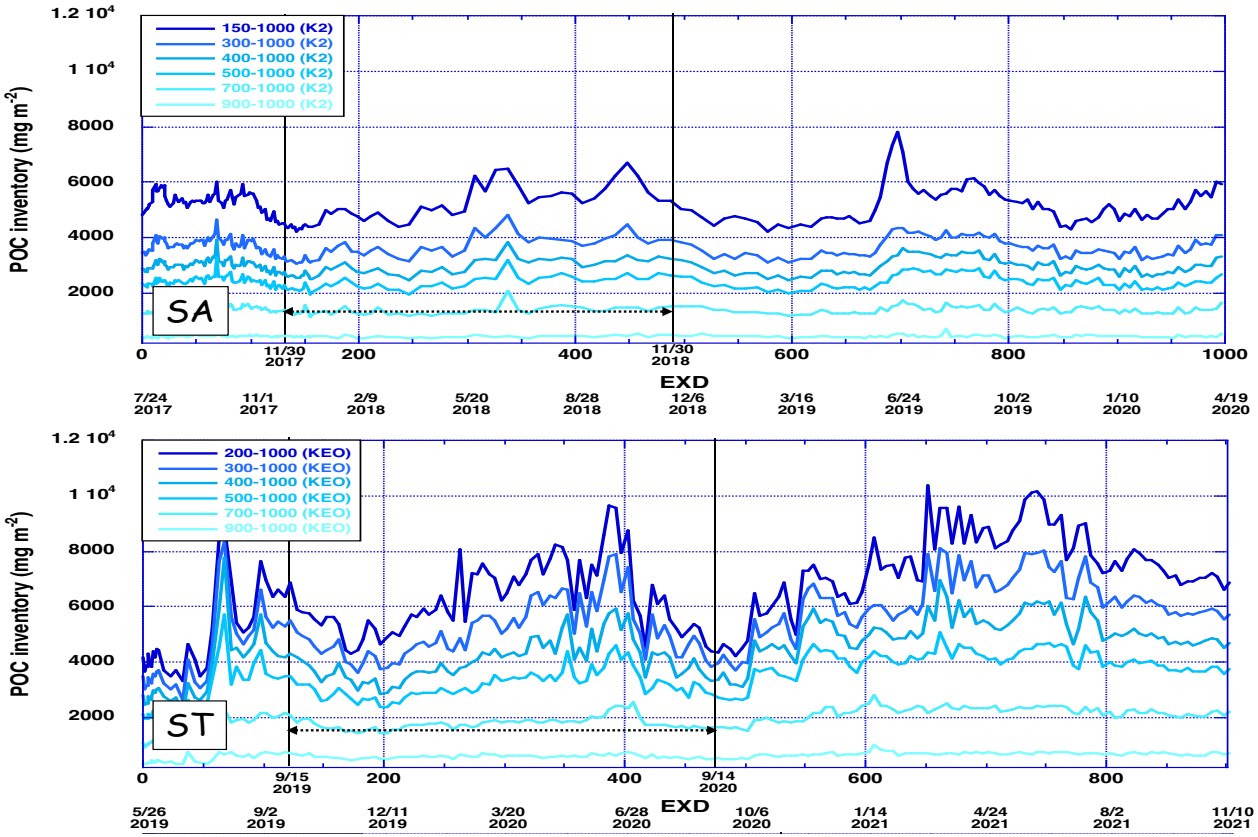

Figure 6 POC inventory between respective depths and 1000 m for (a) subarctic (SA) and (b) subtropical regions. Black broken arrows denote the period when annual POC fluxes were estimated.

8. Backscatter-based POC flux

Assuming the steady state and the same water mass, seasonal variability in oceanography is repeated. If this is the case, difference between annual maximum and minimum POC inventories between the target depth and the reference depth can be regarded as the annual POC flux. POC flux was estimated bellow 150 m for the ST region and 200 m for the ST region. The reference depth was set 1000 m (deepest depth of the ST BGC-Argo measurement) for both regions.

During 30 November 2017 - 30 November 2018 for the SA region and 15 September 2019 – 14 September 2020 for the ST region (Fig. 6), difference between maximum and minimum POC inventory at respective depths were computed as annual POC fluxes at respective depths.

Fig. 7 show annual POC flux at respective depths for respective regions. In the SA region or the WSAG, annual POC flux at 150 m was estimated to be 6.8 mg m^{-2} day^{-1}. POC flux decreased with depth by 0.5 mg m^{-2} day^{-1} at 900 m. In the ST region, annual POC flux at 200 m was estimated to be 14.9 mg m^{-2} day^{-1} and decreased with depth. Annual POC flux at 900 m was estimated to be 0.8 mg m^{-2} day^{-1}.

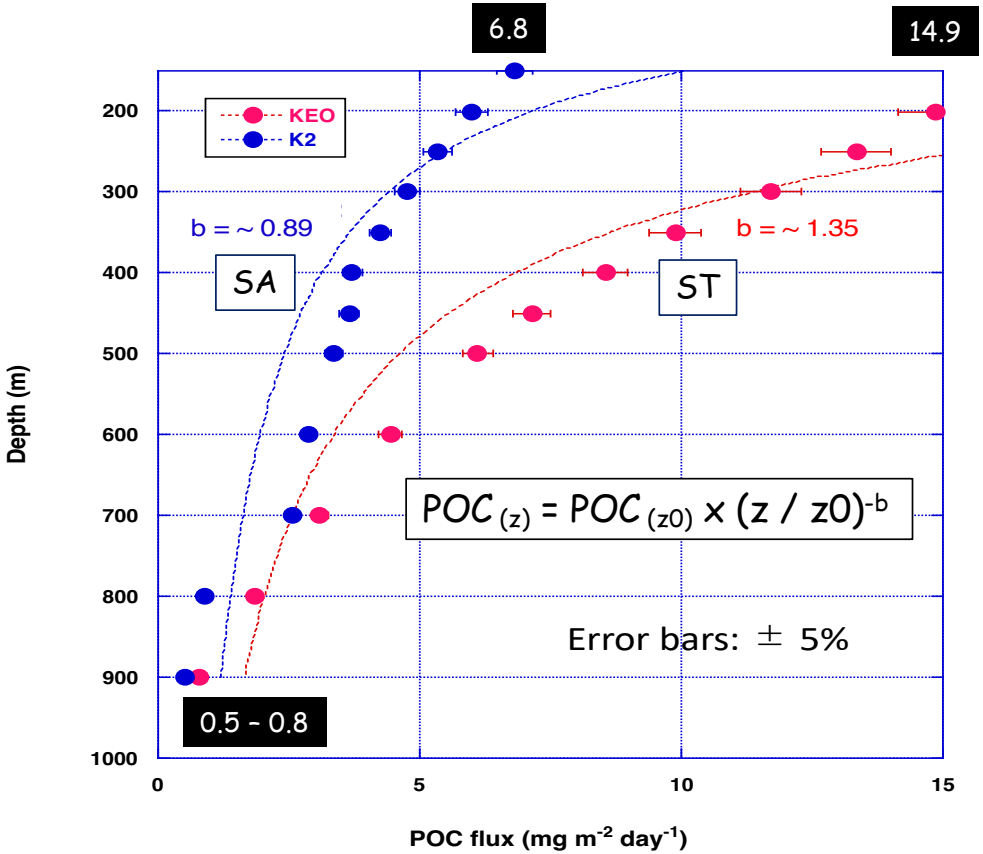

Figure 7 Annual POC flux at respective depths for the subarctic (blue) and subtropical (red) regions. Data are curve-fitted to the power low function (Martin curve). Error bars are 5 % of each data.

9. Sediment trap-based POC flux

Time-series sediment trap observation revealed that POC flux at about 5000 m of station K2 was about 13 mg m^{-2} day^{-1} in July 2017 (~ EXD0) and decreased toward winter. POC flux increased largely by about 25 mg m^{-2} day^{-1} in May 2020 (~ EXD300) (Fig. 8). Relatively higher POC flux was also observed in summer 2021 (~ EXD 750). Average POC flux during the period when backscatter-based annual POC flux was estimated was ~ 5.8 mg m^{-2} day^{-1}. Compared with POC flux at K2, POC flux at KEO was smaller. Average POC flux between September 2019 and August 2020 was estimated to be 4.0 mg m^{-2} day^{-1}. Thus, POC fluxes at about 5000 m observed by moored time-series sediment trap were significantly larger than backscatter-based POC flux at 900 m. Thus, although annual amplitude of POC concentration below 1000 m was ignored this study and estimated POC flux was potentially underestimated, its effect is small and backscatter-based POC flux was likely much smaller than POC flux observed by ordinary sediment trap.

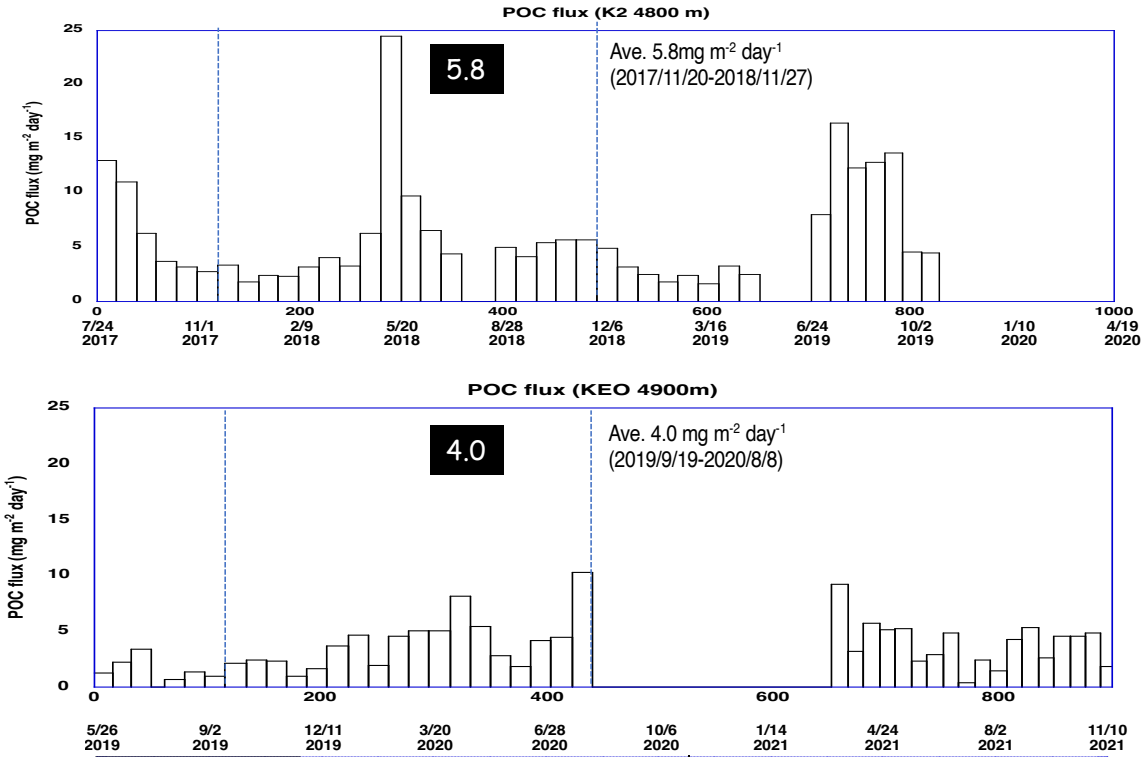

Figure 8 POC flues at about 5000 m observed by time-series sediment trap at stations (a) K2 and (b) KEO. Black broken arrows denote the period when annual POC fluxes were estimated.

10. Summary

Particulate organic carbon (POC) flux in the western North Pacific subarctic and subtropical regions were estimated with backscatter data obtained from two biogeochemical (BGC-) Argo floats. After backscatter data were converted to POC concentration based on the empirical equation, assuming that difference between annual maximum and minimum POC inventories between respective depths and deepest depth (1000 m) is annual POC flux at respective depths under steady state, POC fluxes at respective depths were estimated. POC flux at 150 m for the subarctic region was estimated to be about 6.8 mg m^{-2} day^{-1} and decreased with depth. POC flux at 900 m was estimated to be about 0.5 mg m^{-2} day^{-1}. POC flux at 200 m for the subtropical region was estimated to be about 14.9 mg m^{-2} day^{-1} and decreased with depth by about 0.8 mg m^{-2} day^{-1} at 900 m. These POC fluxes were significantly smaller than those observed by moored sediment trap in these regions. It is likely that backscatter-based POC flux is POC flux by small and slow sinking particles while sediment trap based POC flux is POC flux by large and fast sinking particle. Backscatter based POC flux might fill the gap (mismatch) between carbon supply to and carbon demand in the twilight zone.